Chemistry of *C*-Trimethylsilyl-Substituted Heterocarboranes. 9. Reactivity of *closo*-Germa- and *closo*-Plumbacarboranes toward a Monodentate Lewis Base, (Ferrocenylmethyl)dimethylamine: Synthetic, Structural, and Bonding Studies on the Donor–Acceptor Complexes 1-M[(η^5-C_5H_5)Fe(η^5-$C_5H_4CH_2(Me)_2N$)]-2-($SiMe_3$)-3-R-2,3-$C_2B_4H_4$ (M = Ge, Pb; R = $SiMe_3$, Me, H)

Narayan S. Hosmane,* Kai-Juan Lu, Hongming Zhang, John A. Maguire, Lei Jia, and Reynaldo D. Barreto

Department of Chemistry, Southern Methodist University, Dallas, Texas 75275

Received November 18, 1991

closo-1-Ge-2-($Si(CH_3)_3$)-3-R-2,3-$C_2B_4H_4$ (R = $Si(CH_3)_3$ (I), CH_3 (II), and H (III)) and *closo*-1-Pb-2-($Si(CH_3)_3$)-3-R-2,3-$C_2B_4H_4$ (R = $Si(CH_3)_3$ (VII), CH_3 (VIII), and H (IX)) react with (ferrocenylmethyl)-dimethylamine (ferrocene amine) in dry benzene to give the corresponding donor–acceptor adducts IV–VI and X–XII, respectively, in yields ranging from 56% to 79%. Complex X was converted into two crystal modifications, X(A) and X(B), by slow crystal growth from ferrocene amine and by slow sublimation in vacuo, respectively. The crystal structures of IV, X(A), and X(B) were determined by single-crystal X-ray diffraction. All show that the nitrogen of the ferrocene amine base bonds to the capping metal of the metallacarborane. The metal is not symmetrically bonded to the atoms of the C_2B_3 face but is slipped toward the boron side of the face, giving a distorted-pentagonal-bipyramidal MC_2B_4 cage. Similarities in the NMR and IR spectra of IV–VI and X–XII indicate that all complexes have similar structures. The unit cells of both IV and X(B) contain two crystallographically independent molecules; in one the metal–base nitrogen bond is in the mirror plane of the MC_2B_4 cage, while in the other the bond is slightly rotated out of this plane. The molecules in the unit cell of X(A) are identical. In all structures the ferrocenyl groups are rotated toward the metallacarboranes so that some of the metal–ferrocene distances are within their van der Waals radii. Fenske–Hall molecular orbital calculations show that there are direct interactions between the metal and the Cp(π) orbitals of the ferrocenyl group. It is suggested that the stability gained by such interactions is responsible for the non sterically favorable positions of the ferrocenes. Complexes IV, X(A), and X(B) all crystallized in the triclinic space group $P\bar{1}$ with a = 12.633 (3), 10.106 (3), and 12.677 (3) Å, b = 14.146 (3), 11.179 (3), and 14.308 (4) Å, c = 17.407 (4), 14.218 (4), and 17.348 (6) Å, α = 102.65 (2), 75.92 (2), and 103.02 (2)°, β = 96.63 (2), 70.49 (2), and 97.39 (2)°, γ = 110.85 (2), 70.03 (2), and 110.15 (2)°, V = 2772 (1), 1407.8 (7), and 2803 (1) Å^3, and Z = 4, 2, and 4, respectively. Full-matrix least-squares refinements of IV, X(A), and X(B) converged at R = 0.036, 0.029, and 0.097 and R_w = 0.043, 0.035, and 0.146, respectively.

Introduction

The structural chemistry of the pentagonal-bipyramidal stannacarboranes of the type 1-Sn-2-($Si(CH_3)_3$)-3-R-2,3-$C_2B_4H_4$ (R = $Si(CH_3)_3$, CH_3, H), and their Lewis base complexes, has been extensively investigated.[1,2] Most of the bases reported have been aromatic polydentate nitrogen bases such as 2,2′-bipyridine ($C_{10}H_8N_2$),[3,4] 1,10-phenanthroline ($C_{12}H_8N_2$),[5] 2,2′-bipyrimidine ($C_8H_6N_4$),[6,7] and 2,2′:6′,2″-terpyridine ($C_{15}H_{11}N_3$).[8] There are some questions as to the hapticity of the terpyridine base in the stannacarborane adduct. The X-ray structure shows a unit cell with three independent molecules; tin–nitrogen bond distances indicate that, in each of the isomers, the tin is bonded strongly to only two of the three terpyridine nitrogens.[8] Thus, the terpyridine could be viewed as functioning more as a bidentate ligand than a tridentate one. The structures of all the base–stannacarborane complexes show that coordination by the base induces (or increases) a dislocation, or slippage, of the tin atom toward the boron side of the C_2B_3 face of the carborane and that the base molecules are oriented opposite the cage carbons.

Because of the difficulties in obtaining good single crystals of the small cage complexes, there has been only one structure reported for a monodentate base–stannacarborane complex, the (ferrocenylmethyl)dimethylamine (ferrocene amine) complex 1-Sn[(η^5-C_5H_5)Fe(η^5-$C_5H_4CH_2(CH_3)_2N$)]-2,3-($Si(CH_3)_3$)$_2$-2,3-$C_2B_4H_4$.[7] The X-ray structure shows two independent molecules in the unit cell. In one molecule the Sn–N bond is directly over the unique boron in the C_2B_3 face of the carborane, while in the other isomer the bond is slightly rotated away from this postion. In both molecules the Sn is slipped toward the boron side of the carborane cage, as was found in the bidentate adducts. The most intriguing structural feature of the ferrocene amine complexes is that in both molecules the ferrocenyl groups are not in positions of minimum steric interactions but are in almost eclipsed positions relative to the stannacarboranes, so that some of the cyclopentadienyl carbons are well within the van der Waals

(1) Hosmane, N. S.; Maguire, J. A. In *Molecular Structure and Energetics*; Greenberg, A., Liebman, J. F., Williams, R. E., Eds.; VCH: New York, 1988; Vol. 5, Chapter 14.
(2) Hosmane, N. S.; Maguire, J. A. *Adv. Organomet. Chem.* **1990**, *30*, 99.
(3) Hosmane, N. S.; de Meester, P.; Maldar, N. N.; Potts, S. B.; Chu, S. S. C.; Herber, R. H. *Organometallics* **1986**, *5*, 772.
(4) Siriwardane, U.; Hosmane, N. S.; Chu, S. S. C. *Acta Crystallogr., Sect. C: Cryst. Struct. Commun.* **1987**, *43*, 1067.
(5) Maguire, J. A.; Fagner, J. S.; Siriwardane, U.; Banewicz, J. J.; Hosmane, N. S. *Struct. Chem.* **1990**, *1*, 583.
(6) Hosmane, N. S.; Islam, M. S.; Siriwardane, U.; Maguire, J. A.; Campana, C. F. *Organometallics* **1987**, *6*, 2447.
(7) Hosmane, N. S.; Fagner, J. S.; Zhu, H.; Siriwardane, U.; Maguire, J. A.; Zhang, G.; Pinkston, B. S. *Organometallics* **1989**, *8*, 1769.
(8) Siriwardane, U.; Maguire, J. A.; Banewicz, J. J.; Hosmane, N. S. *Organometallics* **1989**, *8*, 2792.

0276-7333/92/2311-2458$03.00/0

radius of the tin atoms. Thus, it may be that the ferrocene moiety is acting as more than just a pendant group that promotes single-crystal formation. In addition, the change in the ^{119}Sn NMR chemical shift of the stannacarborane on complexation with the ferrocene amine is in the direction opposite from that found for other base–stannacarborane complexes.[7] It has been speculated that an extended C_2B_4–Sn–Cp–Fe–Cp interaction might contribute to this anomalous chemical shift behavior.[7]

There have been only a few reports on structures of base–metallacarborane complexes in the larger cage icosahedral system. Structures of the adducts of the stannacarborane 1,2-$(CH_3)_2$-3,2,1-$SnC_2B_9H_9$ with the bidentate base 2,2′-bipyridine and the monodentate base THF have been reported.[9] Both show a tin slip distortion and base orientation similar to those found in the pentagonal-bipyramidal complexes. Information on the other group 14 metallacarborane–base adducts is even more limited, and what information that is available tends to raise more questions than it answers. Hawthorne and co-workers[10] have reported the reaction of the silacarborane sandwich compound *commo*-3,3′-$Si(C_2B_9H_{11})_2$ with the Lewis bases pyridine and trimethylphosphine. The reaction with pyridine yielded the adduct (10-*exo*-η^1-7,8-$C_2B_9H_{11}$)(10-*endo*-η^1-7,8-$C_2B_9H_{11}$)$Si(C_5H_5N)_2$, in which the $Si(C_5H_5N)_2$ moiety adopts a slipped endo configuration with one of the carbollides but is exopolyhedrally bound to the other carborane unit. The trimethylphosphine did not bond to the silicon but attacked one of the B–H vertices to form a substituted dicarbacanastide cage; the other carbollide unit was bound to the silicon in a slipped endo configuration. In the pentagonal-bipyramidal system, the structures of 1-$(C_{10}H_8N_2)$M-2,3-$(Si(CH_3)_3)_2$-2,3-$C_2B_4H_4$ (M = Ge, Pb) have been determined.[11,12] Although both show metal slippages and base orientations similar to those of the corresponding tin complexes, one metal–nitrogen bond in each complex is significantly shorter than the other. At this point it is not clear why both germanium and lead tend to bond more strongly to only one of two equivalent nitrogens, while tin seems to prefer bidentate coordination, even when more than two base sites are available. Indeed, it is still an open question as to whether the results reported to date reflect actual bonding preferences or are just the consequences of rather flat potential energy surfaces and crystal-packing forces.[5] In an effort to obtain more information regarding the structure and bonding in the group 14 metallacarborane–base complexes, the adducts 1-M[(η^5-C_5H_5)Fe(η^5-$C_5H_4CH_2(CH_3)_2N$)]-2,3-$(Si(CH_3)_3)_2$-2,3-$C_2B_4H_4$ (M = Ge, Pb) were synthesized and structurally characterized. The intracluster bonding was analyzed using Fenske–Hall molecular orbital calculations. The results of this structure–bonding study are reported herein.

Experimental Section

Materials. 2,3-Bis(trimethylsilyl)-2,3-dicarba-1-germa-*closo*-heptaborane(6), 2-(trimethylsilyl)-3-methyl-2,3-dicarba-1-germa-*closo*-heptaborane(6), 2-(trimethylsilyl)-2,3-dicarba-1-germa-*closo*-heptaborane(6), 2,3-bis(trimethylsilyl)-2,3-dicarba-1-plumba-*closo*-heptaborane(6), 2-(trimethylsilyl)-3-methyl-2,3-dicarba-1-plumba-*closo*-heptaborane(6), and 2-(trimethylsilyl)-2,3-dicarba-1-plumba-*closo*-heptaborane(6) were prepared by the methods of Hosmane et al.[10,11] Prior to use, (ferrocenylmethyl)dimethylamine (Strem Chemicals, Inc., Newburyport, MA) was distilled in vacuo. Purity was checked by IR, NMR and boiling point measurements. Benzene and *n*-hexane were dried over $LiAlH_4$ and doubly distilled before use. All other solvents were dried over 4–8 mesh molecular sieves (Aldrich) and either saturated with dry argon or degassed before use.

Spectroscopic Procedures. Proton, boron-11, and carbon-13 pulse Fourier transform NMR spectra, at 200, 64.2, and 50.3 MHz, respectively, were recorded on an IBM-200 SY multinuclear NMR spectrometer. Infrared spectra were recorded on a Perkin-Elmer Model 283 infrared spectrometer and a Perkin-Elmer Model 1600 FT-IR spectrophotometer. Mass spectral determinations were performed by the Midwest Center for Mass Spectrometry, University of Nebraska—Lincoln, Lincoln, NE. Elemental analyses were obtained from Oneida Research Services, Inc., Whitesboro, NY.

Synthetic Procedures. All experiments were carried out in Pyrex glass round-bottom flasks of 250-mL capacity, containing magnetic stirring bars and fitted with high-vacuum Teflon valves. Nonvolatile substances were manipulated in either a drybox or evacuable glovebags under an atmosphere of dry nitrogen. All known compounds among the products were identified by comparing their IR and ^1H NMR spectra with those of authentic samples.

Synthesis of 1-Ge[(η^5-C_5H_5)Fe(η^5-$C_5H_4CH_2(Me)_2N$)]-2-($SiMe_3$)-3-(R)-2,3-$C_2B_4H_4$ (R = $SiMe_3$, Me, H). *closo*-1-Ge-2,3-$(SiMe_3)_2$-2,3-$C_2B_4H_4$ (I; 1.461 g, 5.033 mmol), *closo*-1-Ge-2-($SiMe_3$)-3-(Me)-2,3-$C_2B_4H_4$ (II; 1.14 g, 4.91 mmol), or *closo*-1-Ge-2-($SiMe_3$)-2,3-$C_2B_4H_5$ (III; 0.71 g, 3.26 mmol) was dissolved in freshly distilled dry benzene (20 mL) in vacuo. This solution was then poured under high vacuum onto freshly distilled (anhydrous) (ferrocenylmethyl)dimethylamine, (η^5-C_5H_5)Fe(η^5-$C_5H_4CH_2(Me)_2N$) (1.23 g (5.06 mmol), 1.19 g (4.89 mmol), or 0.79 g (3.25 mmol) when I, II, or III was used), contained in a 100-mL round-bottom flask maintained at −78 °C. When the reaction flask was warmed to 0 °C, the bright orange color of the mixture turned to dark red and the solution became turbid slowly. This mixture was then warmed to room temperature and stirred constantly for 8 days, during which time no gas evolution was detected and the solution became dark brown. The solvent, benzene, and a trace quantity of unreacted (ferrocenylmethyl)-dimethylamine were then removed by pumping the reaction mixture over a period of 18 h in vacuo at room temperature to collect a bright red gummy solid in the flask. The flask containing the gummy solid was then attached to a detachable high-vacuum U-trap which was immersed in an ice bath. With fractional distillation and/or sublimation procedures, temperatures, and times identical with those described for the syntheses of a number of donor–acceptor complexes of *closo*-stanna-, *closo*-germa-, and *closo*-plumbacarborane derivatives,[3,11,12] the gummy solid gave red-orange plates of 1-Ge[(η^5-C_5H_5)Fe(η^5-$C_5H_4CH_2(Me)_2N$)]-2,3-$(SiMe_3)_2$-2,3-$C_2B_4H_4$ (IV; 1.836 g, 3.44 mmol; 68% yield based on I consumed; mp 66–67 °C), orange microcrystals of 1-Ge-[(η^5-C_5H_5)Fe(η^5-$C_5H_4CH_2(Me)_2N$)]-2-($SiMe_3$)-3-(Me)-2,3-$C_2B_4H_4$ (V; 1.296 g, 2.73 mmol; 56% yield base on II consumed; mp 43–44 °C), or a brown liquid of 1-Ge[(η^5-C_5H_5)Fe(η^5-$C_5H_4CH_2(Me)_2N$)]-2-($SiMe_3$)-2,3-$C_2B_4H_5$ (VI; 1.04 g, 2.25 mmol; 69% yield based on III consumed; bp 140–145 °C/10^{-3} mmHg) in the detachable U-trap held at 0 °C. No decomposition products were identified among the material collected in the U-trap. A small quantity of a dark brown residue that remained in the reaction flask after sublimation and/or distillation was discarded because of its insolubility in organic solvents.

The complexes IV–VI are all reasonably soluble in THF, $CHCl_3$, benzene, CH_2Cl_2, and CH_3CN and less soluble in dry *n*-pentane and *n*-hexane. Since the complexes IV–VI all decompose quickly upon brief exposure to air and/or moisture, accurate microanalytical data could not be obtained, even for single-crystal samples. The spectroscopic characterizations of these complexes are presented in Tables I and II.

Synthesis of 1-Pb[(η^5-C_5H_5)Fe(η^5-$C_5H_4CH_2(Me)_2N$)]-2-($SiMe_3$)-3-(R)-2,3-$C_2B_4H_4$ (R = $SiMe_3$, Me, H). In a procedure identical with that employed above, 4.59 mmol (1.95 g) of *closo*-1-Pb-2,3-$(SiMe_3)_2$-2,3-$C_2B_4H_4$ (VII), 3.14 mmol (1.15 g) of *closo*-1-Pb-2-($SiMe_3$)-3-(Me)-2,3-$C_2B_4H_4$ (VIII), or 4.23 mmol (1.49

(9) Jutzi, P.; Galow, P.; Abu-Orabi, S.; Arif, A. M.; Cowley, A. H.; Norman, N. C. *Organometallics* **1987**, *6*, 1024.
(10) Schubert, D. M.; Rees, W. S., Jr.; Knobler, C. B.; Hawthorne, M. F. *Organometallics* **1990**, *9*, 2938.
(11) Hosmane, N. S.; Islam, M. S.; Pinkston, B. S.; Siriwardane, U.; Banewicz, J. J.; Maguire, J. A. *Organometallics* **1988**, *7*, 2340.
(12) Hosmane, N. S.; Lu, K.-J.; Zhu, H.; Siriwardane, U.; Shet, M. S.; Maguire, J. A. *Organometallics* **1990**, *9*, 808.

Table I. FT NMR Spectral Data[a]

compd	δ, splitting, assignt ($^1J(^{11}B-^1H)$ or $^1J(^{13}C-^1H)$, Hz)	rel area
	200.13-MHz ^1H NMR Data[b]	
IV	4.91, q (br), basal H_t (145); 4.12, s, C_5H_4; 4.09, s, C_5H_5; 3.28, s, CH_2; 2.87, q (br), apical H_t (164); 2.13, s, $N(Me)_2$; 0.41, s, $SiMe_3$	3:4:5:2:1:6:18
V	4.83, q (br), basal H_t (143); 4.19, q (br), basal H_t (122); 4.09, s, C_5H_4; 4.03, s, C_5H_5; 3.29, s, CH_2; 2.67, q (br), apical H_t (146); 2.57, s, C_{cage}–Me; 2.09, s, $N(Me)_2$; 0.29, s, $SiMe_3$	1:2:4:5:2:1:3:6:9
VI	6.53, s (br), C_{cage}–H; 5.03, q (br), basal H_t (137); 3.98, q (br), basal H_t (unresolved); 3.43, s, C_5H_4; 3.38, s, C_5H_5; 2.63, s, CH_2; 2.57, q (br), apical H_t (154); 1.42, s, $N(Me)_2$; –0.42, s, $SiMe_3$	1:1:2:4:5:2:1:6:9
X	5.92, q (br), basal H_t (123); 5.36, q (br), basal H_t (unresolved); 4.04, s, C_5H_4; 3.94, s, C_5H_5; 3.24, s, CH_2; 2.63, q (br), apical H_t (159); 1.88, s, $N(Me)_2$; 0.49, s, $SiMe_3$	1:2:4:5:2:1:6:18
XI	6.22, q (br), basal H_t (unresolved); 5.87, q (br), basal H_t (unresolved); 4.12, s, C_5H_4; 4.05, s, C_5H_5; 3.40, s, CH_2; 3.28, q (br), apical H_t (143); 2.56, s, C_{cage}–Me; 2.20, s, $N(Me)_2$; 0.26, s, $SiMe_3$	1:2:4:5:2:1:3:6:9
XII	6.62, s (br), C_{cage}–H; 5.66, q (br), basal H_t (111); 4.99, q (br), basal H_t (unresolved); 4.18, s, C_5H_4; 4.10, s, C_5H_5; 3.51, s, CH_2; 2.85, q (br), apical H_t (140); 2.30, s, $N(Me)_2$; 0.23, s, $SiMe_3$	1:1:2:4:5:2:1:6:9
	64.21-MHz ^{11}B NMR Data[c]	
IV	18.85, d, basal BH (144); –7.83, d, apical BH (164)	3:1
V	18.07, d, basal BH (143); 12.34, d, basal BH (122); –9.62, d, apical BH (146)	1:2:1
VI	23.49, d (br), basal BH (137); 14.41, ill-defined broad peak, basal BH (unresolved); –9.53, d (br), apical BH (154)	1:2:1
X	26.52, d (br), basal BH (127); 20.96, ill-defined broad peak, basal BH (unresolved); –10.78, d (br), apical BH (159)	1:2:1
XI	38.94, ill-defined very broad peak, basal BH (unresolved); 24.14, ill-defined very broad peak, basal BH (unresolved); –2.55, d (v br), apical BH (143)	1:2:1
XII	39.61, d (br), basal BH (111); 21.72, ill-defined broad peak, basal BH (unresolved); –5.99, d (br), apical BH (140)	1:2:1
	50.32-MHz ^{13}C NMR Data[b,d]	
IV	136.23, s (br), cage C (SiCB); 82.7, s, ferrocenyl C; 70.10, d, ferrocenyl CH (174); 68.39, d, C_5H_5 (169); 67.96, d, ferrocenyl CH (168); 58.99, t, CH_2 (135); 44.57, q, $(Me)_2N$ (130); 1.69, q, $SiMe_3$ (121)	2:1:2:5:2:1:2:6
V	137.81, s (br), cage C (SiCB); 131.71, s (br), cage C (CCB); 81.46, s, ferrocenyl C; 69.86, d, ferrocenyl CH (176); 68.10, d, C_5H_5 (174); 67.79, d, ferrocenyl CH (176); 58.40, t, CH_2 (136); 43.96, q, $(Me)_2N$ (134); 22.56, q (br), C_{cage}–Me (129); 0.18, q, $SiMe_3$ (120)	1:1:1:2:5:2:1:2:1:3
VI	132.53, s (br), cage C (SiCB); 122.13, d (br), cage CH (194); 81.71, s, ferrocenyl C; 70.13, d, ferrocenyl CH (175); 68.32, d, C_5H_5 (176); 67.96, d, ferrocenyl CH (176); 58.73, t, CH_2 (139); 44.36, q, $(Me)_2N$ (139); –1.17, q, $SiMe_3$ (121)	1:1:1:2:5:2:1:2:3
X	135.94, s (br), cage C (SiCB); 80.47, s, ferrocenyl C; 70.93, d, ferrocenyl CH (174); 68.93, d, C_5H_5 (179); 58.77, t, CH_2 (138); 44.32, q, $(Me)_2N$ (134); 2.52, q, $SiMe_3$ (119)	2:1:4:5:1:2:6
XI	127.57, s (br), cage C (SiCB); 122.42, s (br), cage C (CCB); 81.63, s, ferrocenyl C; 69.80, d, ferrocenyl CH (175); 68.14, d, C_5H_5 (176); 67.92, d, ferrocenyl CH (176); 58.60, t, CH_2 (135); 44.47, q, $(Me)_2N$ (130); 22.82, q (br), C_{cage}–Me (127); 0.81, q, $SiMe_3$ (120)	1:1:1:2:5:2:1:2:1:3
XII	123.35, s (br), cage C (SiCB); 111.62, d (br), cage CH (163); 80.27, s, ferrocenyl C; 70.19, d, ferrocenyl CH (181); 68.66, d, C_5H_5 (176); 68.55, d, ferrocenyl CH (176); 58.81, t, CH_2 (137); 44.99, q, $(Me)_2N$ (135); –0.51, q, $SiMe_3$ (120)	1:1:1:2:5:2:1:2:3

[a] $CDCl_3$ was used as solvent and an internal standard of δ 7.23 ppm (in the ^1H NMR spectra) and δ 77.0 ppm (in the ^{13}C NMR spectra), with a positive sign indicating a downfield shift. Legend: s = singlet, d = doublet, t = triplet, q = quartet. [b] Shifts relative to external Me_4Si. [c] Shifts relative to external $BF_3 \cdot OEt_2$. [d] Since relaxation of carbon without H is much slower than that of a CH unit, the relative areas of cage carbons as well as one of the ferrocenyl carbons could not be measured accurately.

g) of *closo*-1-Pb-2-($SiMe_3$)-2,3-$C_2B_4H_5$ (IX) was reacted with anhydrous (ferrocenylmethyl)dimethylamine, (η^5-C_5H_5)Fe(η^5-$C_5H_4CH_2(Me)_2N$) (1.12 g (4.60 mmol), 0.764 g (3.14 mmol), or 1.03 g (4.24 mmol) when VII, VIII, or IX was used), in dry benzene over a period of 7 days to isolate the yellow-orange, crystalline solid 1-Pb[(η^5-C_5H_5)Fe(η^5-$C_5H_4CH_2(Me)_2N$)]-2,3-$(SiMe_3)_2$-2,3-$C_2B_4H_4$ (X; 2,436 g, 3.65 mmol; 79% yield based on VII consumed; mp 94–95 °C), a reddish brown liquid (low-melting solid, mp 28 °C) of 1-Pb[(η^5-C_5H_5)Fe(η^5-$C_5H_4CH_2(Me)_2N$)]-2-($SiMe_3$)-3-(Me)-2,3-$C_2B_4H_4$ (XI; 1.296 g, 2.13 mmol; 68% yield based on VIII consumed; bp 120–130 °C/10^{-3} mmHg), or orange plates of 1-Pb[(η^5-C_5H_5)Fe(η^5-$C_5H_4CH_2(Me)_2N$)]-2-($SiMe_3$)-2,3-$C_2B_4H_5$ (XII; 1.49 g, 2.50 mmol; 59% yield based on IX consumed; mp 133–134 °C) as the only sublimed or distilled reaction product on the inside walls of the detachable U-trap. The side arms of both the reaction flask and the U-trap were maintained at 140–150 °C with heating tape during the sublimation. A trace quantity of unreacted (ferrocenylmethyl)dimethylamine was recovered in a trap held at –196 °C during the mild sublimation of the yellow-orange reaction residue. The plumbacarborane precursors and their product of decomposition, elemental lead (Pb^0), were not identified in the sublimate. A substantial quantity of a dark brown residue that remained in the reaction flask after sublimation was discarded because of its insolubility in organic solvents.

The complexes X–XII are all reasonably soluble in THF, $CHCl_3$, benzene, CH_2Cl_2, and CH_3CN and less soluble in dry *n*-pentane and *n*-hexane. Since complex XII decomposes quickly upon brief exposure to air and/or moisture, accurate microanalytical data could not be obtained, even for single-crystal samples. Anal. Calcd. for $C_{21}H_{39}BNSi_2FePb$ (X): C, 37.76; H, 5.88; N, 2.10. Found: C, 37.57; H, 5.82; N, 2.04. Calcd for $C_{19}H_{33}B_4NSiPbFe$ (XI): C, 37.42; H, 5.45; N, 2.30. Found: C, 38.85; H, 5.51; N, 2.33. The spectroscopic characterizations of these complexes are presented in Tables I and II.

Crystal Structure Analyses of 1-Ge[(η^5-C_5H_5)Fe(η^5-$C_5H_4CH_2(Me)_2N$)]-2,3-$(SiMe_3)_2$-2,3-$C_2B_4H_4$ (IV) and 1-Pb-[(η^5-C_5H_5)Fe(η^5-$C_5H_4CH_2(Me)_2N$)]-2,3-$(SiMe_3)_2$-2,3-$C_2B_4H_4$ (X). While orange crystals of both IV and X(B) were grown by vacuum sublimation onto glass surfaces in 8-mm tubes, yellow-orange crystals of X(A) were obtained by dissolving the crystals of X in a minimum quantity of anhydrous hot ferrocene amine, followed by slowly removing ferrocene amine in vacuo at room temperature over a period of several days and then washing the resulting crystals in vacuo with anhydrous *n*-hexane until all the contaminated ferrocene amine was removed. Since the crystals changed to opaque white upon brief exposure to air, they were sealed in glass capillaries under a N_2 atmosphere and were mounted on a Nicolet R3m/V diffractometer. Final unit cell parameters, given in Table III and supplementary table S-2, were obtained by a least-squares fit of 24 accurately centered reflections measured in the ranges of 15° < 2θ < 25°, 17° < 2θ < 30°, and 18° < 2θ < 25° for IV, X(A), and X(B), respectively. Intensity data were collected at 230 K in the ranges of 3.5° ≤ 2θ ≤ 42°, 3.5° ≤ 2θ ≤ 42°, and 3.5° ≤ 2θ ≤ 40° for IV, X(A), and X(B), respectively. Three standard reflections, monitored after every 150 reflections, did not show any significant change in intensity during the data

Table II. Infrared Absorptions (cm^{-1}; C_6D_6 vs C_6D_6)[a]

compd	absorption
IV	3093 (ms), 2953 (vvs), 2895 (vs), 2856 (ms), 2808 (ms), 2765 (vs) [ν(C–H)], 2560 (vvs) [ν(B–H)], 2226 (ws), 2165 (ms), 1450 (ms), 1402 (ms), 1346 (vs), 1250 (vvs), 1170 (vs), 1100 (vs), 1035 (ms), 1020 (ms), 1010 (ms), 998 (ms), 925 (mbr), 835 (vvs), 815 (sh), 620 (ms), 503 (ms), 490 (ws), 477 (ms), 402 (vs), 380 (vs), 355 (sh)
V	3092 (vs), 2930 (vvs), 2893 (sh), 2847 (sh), 2805 (ms), 2762 (vs) [ν(C–H)], 2540 (vvs) [ν(B–H)], 2188 (vs), 1630 (wbr), 1505 (ms), 1445 (ms), 1400 (ms), 1242 (vs), 1167 (ms), 1132 (ws), 1102 (ms), 1045 (ws), 1020 (sh), 1010 (sh), 998 (vs), 825 (vvs), 620 (ms), 490 (sh), 478 (vvs), 415 (ms), 372 (ws)
VI	3081 (ms), 2953 (vvs), 2899 (sh), 2867 (sh), 2824 (ws), 2782 (ms) [ν(C–H)], 2557 (vvs) [ν(B–H)], 2376 (wbr), 2247 (vs), 2188 (ws), 1792 (ws), 1643 (wbr), 1509 (ms), 1466 (vs), 1402 (vs), 1349 (ws), 1247 (vs), 1167 (ms), 1130 (ws), 1103 (ms), 1071 (ws), 1039 (ws), 1018 (ws), 996 (ws), 906 (vvs), 831 (vvs), 735 (vvs), 649 (vs), 617 (ws)
X	2940 (vvs), 2895 (vs), 2813 (sh), 2792 (sh) [ν(C–H)], 2510 (vvs) [ν(B–H)], 1460 (sh), 1402 (mbr), 1340 (mbr), 1242 (vvs), 1190 (ws), 1095 (ms), 1022 (ms), 987 (vs), 920 (ws), 820 (vvs), 748 (vs), 678 (ms), 618 (ms), 394 (vs), 290 (wbr)
XI	3049 (vs), 2940 (vvs), 2858 (vs), 2810 (vs), 2779 (vs) [ν(C–H)], 2557 (sh), 2520 (vvs) [ν(B–H)], 2259 (ms), 2240 (ws), 1682 (ms), 1445 (mbr), 1400 (ms), 1345 (mbr), 1240 (vs), 1165 (ms), 1131 (ms), 1098 (ms), 1051 (ws), 1032 (ws), 1018 (ws), 995 (ws), 920 (mbr), 830 (vvs), 671 (ws), 618 (vs), 540 (ws), 501 (vs), 490 (vs), 470 (vs), 450 (ws), 407 (vs), 325 (ws), 265 (mbr)
XII	3083 (ms), 2954 (vs), 2884 (ms), 2837 (ms), 2801 (ms) [ν(C–H)], 2531 (vvs) [ν(B–H)], 2238 (ms), 1702 (wbr), 1461 (vs), 1407 (ms), 1343 (ms), 1247 (vs), 1173 (ms), 1138 (ms), 1102 (ms), 1067 (ms), 1021 (ms), 991 (ms), 914 (ws), 832 (vvs), 749 (ms), 709 (ms), 685 (ws), 620 (ms), 509 (sh), 479 (vs)

[a] Legend: v = very, s = strong or sharp, m = medium, w = weak, sh = shoulder, br = broad.

collection. These data were corrected for Lorentz and polarization effects. The semiempirical absorption correction method was applied; the minimum and maximum transmission factors for IV, X(A), and X(B) are 0.6175 and 0.7940, and 0.6175 and 1.0000, and 1.0000 and 0.9042, respectively. The structures were solved by direct methods stored in the SHELXTL-Plus package.[13] All non-H atoms of IV and X(A) were refined anisotropically. However, due to the poor quality of the data set for X(B), only Pb was anisotropically refined, and the remaining non-H atoms were refined isotropically. A number of attempts were made to resolve the problems associated with the analysis of X(B). Diffraction data were collected from three different preparations of X; the possibilities of other space groups and/or cell populations were thoroughly investigated. All studies yielded the same results, that is, a $P\bar{1}$ space group and large values of R. The poor fit arises from problems resulting from the very intense scattering of the four lead atoms in the unit cell of X(B) ($Z = 4$), rather than poor crystal quality, incorrect structure assignments, or absorption problems. When X was recrystallized under milder conditions, the solid modification X(A) was obtained that had a lower unit cell population, $Z = 2$, and a much smaller R factor ($R_w = 0.035$). Since the internal 1-Pb[(η^5-C_5H_5)Fe(η^5-$C_5H_4CH_2(CH_3)_2N$)]-2,3-$(Si(CH_3)_3)_2$-2,3-$C_2B_4H_4$ geometries of X(A) and X(B) are essentially the same, the inclusion of X(B) in this report would add little to our understanding of the bonding in these systems and its crystallographic data are included only in the supplementary material (see supplementary tables S-2–S-5 and S-9). Full-matrix least-squares refinements were performed on IV, X(A), and X(B). Scattering factors with corrections for anomalous dispersion were taken from ref 14. Hydrogen atoms of IV and X(A), located on

Table III. Crystallographic Data[a] for IV and X(A)

	IV	X(A)
formula	$C_{21}H_{39}B_4NSi_2GeFe$	$C_{21}H_{39}B_4NSi_2PbFe$
fw	533.39	668.00
cryst syst	triclinic	triclinic
space group	$P\bar{1}$	$P\bar{1}$
a, Å	12.633 (3)	10.106 (3)
b, Å	14.146 (3)	11.179 (3)
c, Å	17.407 (4)	14.218 (4)
α, deg	102.65 (2)	75.92 (2)
β, deg	96.63 (2)	70.49 (2)
γ, deg	110.85 (2)	70.03 (2)
V, Å^3	2772 (1)	1407.8 (7)
Z	4	2
D_{calcd}, g cm^{-3}	1.278	1.576
cryst dmns, mm	0.30 × 0.20 × 0.15	0.30 × 0.20 × 0.20
scan type	$\theta/2\theta$	$\theta/2\theta$
scan sp in ω deg s^{-1}: min, max	5.0, 30.0	6.0, 30.0
2θ range, deg	3.5–42.0	3.5–42.0
no. of data collected	6009	3263
T, K	230	230
decay, %	0	0
no. of obsd rflns, $I > 3.0\sigma(I)$	4560	2615
no. of params refined	541	271
GOF	1.84	1.17
R[b]	0.036	0.029
R_w	0.043	0.035
$\Delta\rho$, e/Å^3 max, min	0.50, −0.44	0.99, −1.15
k[c]	0.000 20	0.0005
abs coeff, mm^{-1}	1.777	6.625
data/param ratio	8.4:1	9.6:1

[a] Graphite-monochromatized Mo Kα radiation; $\lambda = 0.710\,73$ Å. [b] $R = \sum||F_o| - |F_c||/\sum|F_o|$; $R_w = [\sum w(F_o - F_c)^2/\sum w(F_o)^2]^{1/2}$. [c] $w = 1/[\sigma^2(F_o) + k(F_o)^2]$.

calculated positions, were included without refinement in the structure factor calculation at fixed isotropic temperature factors ($U = 0.08$ Å^2). No attempts were made to find the hydrogen atoms of X(B). The function minimized was $\sum w(|F_o| - |F_c|)^2$. In the final stages of refinement a weighting scheme was used (see Table III). The ratios of largest parameter shifts to their estimated standard deviations were less than 0.01. The final atomic coordinates are listed in Table IV. Selected bond lengths and bond angles are presented in Table V. Mean deviations and dihedral angles of the least-squares planes in IV and X(A) are given in Table VI.

Calculations. Molecular orbital calculations were carried out on the model compounds 1-M[(η^5-C_5H_5)Fe(η^5-$C_5H_4CH_2$-$(CH_3)_2N$)]-2,3-$C_2B_4H_6$ (M = Ge (XIII), Pb (XIV), Sn (XV)), using the unparameterized Fenske–Hall method.[15] The basis functions used were those generated by the numerical Xα atomic orbital program of Herman and Skillman,[16] used in conjunction with the Xα-to-Slater program of Bursten and Fenske.[17,18] Except where noted below, the heavy-atom positions for XIII and XIV were those of molecules IV and X (averaged values), respectively, while those of XV were taken from the X-ray structure of 1-Sn[(η^5-C_5H_5)Fe(η^5-$C_5H_4CH_2(CH_3)_2N$)]-2,3-$(Si(CH_3)_3)_2$-2,3-$C_2B_4H_4$.[7] The unit cells of all the sublimed group 14 metallacarborane–ferrocene amine complexes contain two crystallographically independent molecules. In one (isomer 1) the metal–nitrogen bond is in the mirror plane of the MC_2B_4 cage, that is, directly over the unique boron (B(4) in Figure 1 and supplementary figure S-2B), while in the other, less symmetric molecule (isomer 2), the bond is rotated slightly out of the plane (see below). Most calculations were carried out on the more symmetric isomers. However, the conclusions drawn from the calculations are equally valid for both

(13) Sheldrick, G. M. *Structure Determination Software Programs*; Nicolet Instrument Corp.: Madison, WI, 1988.
(14) *International Tables for X-ray Crystallography*; Kynoch Press: Birmingham, U.K., 1974; Vol. IV.
(15) Hall, M. B.; Fenske, R. F. *Inorg. Chem.* **1972**, *11*, 808.
(16) Herman, F.; Skillman, S. *Atomic Structure Calculations*; Prentice-Hall: Englewood, NJ, 1963.
(17) (a) Bursten, B. E.; Fenske, R. F. *J. Chem. Phys.* **1977**, *67*, 3138. (b) Bursten, B. E.; Jensen, R. J.; Fenske, R. E. *J. Chem. Phys.* **1978**, *68*, 3320.
(18) We wish to thank Prof. M. B. Hall, Texas A&M University, for furnishing a copy of this program.

Table IV. Atomic Coordinates (×10⁴) and Equivalent Isotropic Displacement Coefficients (Å² × 10³)

	x	y	z	U(eq)[a]		x	y	z	U(eq)[a]
				Compound IV					
Ge(1)	1627 (1)	1974 (1)	2137 (1)	42 (1)	Ge(2)	3403 (1)	7618 (1)	2707 (1)	42 (1)
Fe(1)	2378 (1)	1991 (1)	5107 (1)	40 (1)	Fe(2)	2593 (1)	7755 (1)	-396 (1)	41 (1)
Si(11)	4773 (1)	4058 (1)	2330 (1)	54 (1)	Si(21)	2846 (1)	7300 (1)	4930 (1)	44 (1)
Si(12)	2411 (2)	3478 (1)	454 (1)	50 (1)	Si(22)	287 (2)	5798 (1)	3078 (1)	64 (1)
N(1)	252 (4)	561 (3)	2603 (3)	47 (2)	N(2)	4747 (4)	8705 (3)	2072 (2)	46 (2)
C(11)	3492 (4)	2825 (4)	1786 (3)	38 (2)	C(21)	2579 (4)	7614 (4)	3953 (3)	34 (2)
C(12)	2561 (4)	2600 (4)	1089 (3)	39 (2)	C(22)	1588 (4)	7057 (4)	3265 (3)	41 (2)
B(13)	1686 (6)	1410 (5)	822 (4)	48 (3)	B(23)	1634 (6)	7699 (6)	2630 (4)	52 (3)
B(14)	2195 (6)	823 (5)	1420 (4)	55 (4)	B(24)	2765 (6)	8862 (5)	3031 (4)	52 (3)
B(15)	3329 (6)	1804 (5)	2073 (4)	47 (3)	B(25)	3403 (5)	8710 (5)	3875 (4)	44 (3)
B(16)	3188 (6)	1690 (5)	1022 (4)	50 (3)	B(26)	1886 (6)	8369 (5)	3662 (4)	47 (3)
C(117)	5863 (6)	3733 (6)	2873 (5)	132 (5)	C(217)	2720 (8)	5974 (5)	4815 (5)	158 (6)
C(118)	4303 (6)	4861 (5)	3092 (4)	98 (4)	C(218)	4346 (5)	8142 (5)	5485 (4)	89 (4)
C(119)	5527 (6)	4823 (6)	1687 (4)	125 (5)	C(219)	1901 (7)	7629 (8)	5577 (5)	160 (8)
C(120)	2663 (8)	4796 (5)	1085 (4)	120 (5)	C(220)	-725 (9)	5642 (9)	2260 (7)	399 (13)
C(121)	907 (5)	2926 (6)	-145 (4)	90 (4)	C(221)	636 (8)	4684 (6)	2888 (7)	275 (10)
C(122)	3379 (6)	3534 (6)	-262 (4)	98 (5)	C(222)	-447 (7)	5784 (8)	3922 (6)	240 (9)
C(123)	1604 (4)	1615 (4)	3921 (3)	38 (3)	C(223)	3409 (5)	7869 (4)	723 (3)	41 (3)
C(124)	1297 (5)	2377 (5)	4405 (3)	57 (3)	C(224)	2180 (5)	7411 (4)	636 (3)	47 (3)
C(125)	2331 (7)	3268 (5)	4792 (4)	69 (4)	C(225)	1742 (5)	6486 (5)	-14 (3)	54 (3)
C(126)	3257 (6)	3058 (5)	4559 (4)	69 (4)	C(226)	2669 (6)	6363 (5)	-338 (3)	56 (3)
C(127)	2810 (5)	2040 (5)	4022 (3)	51 (3)	C(227)	3712 (5)	7224 (4)	115 (3)	52 (3)
C(128)	1749 (5)	693 (5)	5501 (3)	54 (3)	C(228)	1954 (7)	8843 (5)	-575 (3)	62 (4)
C(129)	1585 (6)	1532 (5)	5994 (3)	57 (3)	C(229)	1429 (6)	7903 (5)	-1220 (3)	57 (3)
C(130)	2709 (6)	2345 (5)	6326 (3)	65 (3)	C(230)	2315 (6)	7732 (5)	-1579 (3)	58 (3)
C(131)	3536 (6)	2010 (5)	6029 (3)	62 (3)	C(231)	3382 (6)	8558 (5)	-1149 (4)	61 (3)
C(132)	2933 (6)	965 (5)	5512 (3)	57 (3)	C(232)	3149 (7)	9231 (5)	-539 (4)	64 (4)
C(133)	818 (4)	549 (4)	3390 (3)	45 (3)	C(233)	4209 (5)	8879 (4)	1330 (3)	48 (3)
C(134)	-677 (5)	951 (5)	2699 (3)	67 (3)	C(234)	5487 (5)	8130 (5)	1877 (3)	67 (3)
C(135)	-240 (5)	-509 (5)	2055 (3)	74 (3)	C(235)	5455 (5)	9744 (5)	2639 (3)	67 (3)
				Compound X(A)					
Pb	8281 (1)	9241 (1)	7677 (1)	39 (1)	C(11)	10330 (11)	13732 (8)	6192 (8)	80 (6)
Fe	4297 (1)	7333 (1)	7997 (1)	37 (1)	C(12)	11704 (11)	11763 (11)	7677 (8)	84 (6)
Si(1)	7259 (2)	12728 (2)	5799 (2)	42 (1)	C(13)	6058 (8)	7477 (7)	8303 (5)	36 (3)
Si(2)	10691 (2)	12001 (2)	6744 (2)	46 (1)	C(14)	5219 (8)	8707 (7)	7947 (6)	37 (4)
N	7883 (7)	7277 (6)	9156 (5)	43 (3)	C(15)	5163 (8)	8691 (8)	6981 (6)	47 (4)
C(1)	7647 (8)	11805 (7)	7010 (5)	36 (3)	C(16)	5966 (8)	7470 (8)	6705 (6)	46 (4)
C(2)	8976 (8)	11487 (7)	7369 (5)	36 (3)	C(17)	6516 (8)	6716 (7)	7523 (6)	41 (4)
B(3)	8746 (10)	10780 (9)	8492 (6)	39 (4)	C(18)	3097 (10)	6516 (9)	9291 (6)	55 (5)
B(4)	6962 (10)	10771 (9)	8888 (7)	47 (4)	C(19)	2255 (9)	7735 (9)	8982 (8)	62 (5)
B(5)	6364 (10)	11403 (9)	7859 (7)	44 (4)	C(20)	2155 (9)	7767 (9)	8007 (8)	64 (5)
B(6)	7359 (10)	12185 (9)	8204 (6)	42 (4)	C(21)	2961 (9)	6527 (9)	7719 (7)	56 (4)
C(7)	6486 (12)	14476 (8)	5867 (8)	75 (5)	C(22)	3518 (9)	5767 (8)	8521 (6)	50 (4)
C(8)	8883 (10)	12438 (10)	4679 (6)	74 (5)	C(23)	6441 (8)	7106 (8)	9285 (6)	43 (4)
C(9)	5870 (10)	12159 (9)	5570 (7)	65 (5)	C(24)	8009 (10)	7420 (9)	10123 (6)	64 (5)
C(10)	11929 (9)	10975 (9)	5757 (7)	65 (4)	C(25)	9071 (8)	6181 (8)	8765 (7)	58 (4)

[a] Equivalent isotropic U defined as one-third of the trace of the orthogonalized U_{ij} tensor.

isomers. The X-ray structures of all the complexes showed that the two cyclopentadienyl (Cp) rings in the ferrocene moiety were parallel and twisted away from an eclipsed position by about 7°.[19] In the calculations the Cp rings were assumed to be eclipsed; that is, the base is derived from a ferrocene molecule having D_{5h} symmetry. The positions of the hydrogens relative to the heavy atoms of the carborane were the MNDO optimized positions calculated[20] for [*nido*-2,3-$C_2B_4H_6$]$^{2-}$, and the C–H bond distances in the Cp rings were set at 1.082 Å, with idealized bond angles. For the methyl groups, the carbons were assumed to be tetrahedral and the C–H distances were taken as 0.9604 Å.

Results and Discussion

Synthesis. The donor–acceptor complexes 1-M[(η^5-C_5H_5)Fe(η^5-$C_5H_4CH_2N(CH_3)_2$)]-2-($Si(CH_3)_3$)-3-R-2,3-$C_2B_4H_4$ (M = Ge, Pb; R = $Si(CH_3)_3$, CH_3, H) were synthesized in yields ranging from 56% to 79% by the direct reaction of benzene solutions of the particular metallacarborane with the ferrocene amine base. The extremely long reaction times (7–8 days) required to reach completion, as measured by the solution color and NMR spectra, are somewhat surprising for reactions that seem to involve straightforward adduct formation between free metallacarborane and base molecules. The *closo*-germa- and *closo*-plumbacarboranes (I–III and VII–IX, respectively) are known to react more slowly than do the corresponding stannacarboranes in forming bipyridine complexes[11,12] and the formation of the ferrocene amine–stannacarborane complex was found to be uniquely slow in the tin system.[7] Therefore, the long reaction times needed for the formation of IV–VI and X–XII are likely the consequence of combining slowly reacting acids with a slowly reacting base, rather than some unusual activation process occurring in the reaction.

The colors of the complexes range from orange to red-brown, indicating the presence of charge-transfer transitions in complexes IV–VI and X–XII; such transitions have been found in all the base–group 14 metallacarborane complexes.[3,7,11,12] The melting points of the ferrocene amine–germacarborane complexes decrease monotonically with molar mass, as would be expected for monomeric adduct formation. This is consistent with the X-ray

(19) The twist angles are as follows: for IV, 7.9°; for X, 6.4°; for XIII, 7.0°.[7]

(20) Maguire, J. A.; Ford, G. P.; Hosmane, N. S. *Inorg. Chem.* 1988, *27*, 3354.

Table V. Selected Bond Lengths (Å) and Bond Angles (deg)

Bond Lengths							
Compound IV							
Ge(1)–Cnt(1)[a]	1.893	Ge(1)–C(11)	2.452 (6)	Ge(2)–C(21)	2.512 (6)	Ge(1)–C(22)	2.526 (6)
Ge(1)–C(12)	2.443 (6)	Ge(1)–B(13)	2.272 (7)	Ge(2)–B(23)	2.268 (8)	Ge(2)–B(24)	2.178 (9)
Ge(1)–B(14)	2.208 (8)	Ge(1)–B(15)	2.260 (8)	Ge(2)–B(25)	2.269 (6)	Ge(2)–N(2)	2.406 (6)
Ge(1)–N(1)	2.496 (6)	C(11)–C(12)	1.480 (7)	C(21)–C(22)	1.470 (6)	C(21)–B(25)	1.575 (8)
C(11)–B(15)	1.584 (10)	C(11)–B(16)	1.733 (8)	C(21)–B(26)	1.721 (10)	C(22)–B(23)	1.570 (10)
C(12)–B(13)	1.577 (7)	C(12)–B(16)	1.727 (10)	C(22)–B(26)	1.715 (9)	B(23)–B(24)	1.681 (8)
B(13)–B(14)	1.670 (12)	B(13)–B(16)	1.769 (10)	B(23)–B(26)	1.771 (9)	B(24)–B(25)	1.685 (10)
B(14)–B(15)	1.669 (8)	B(14)–B(16)	1.741 (10)	B(24)–B(26)	1.730 (10)	B(25)–B(26)	1.773 (10)
B(15)–B(16)	1.783 (10)	Ge(2)–Cnt(2)	1.925				
Compound X(A)							
Pb–Cnt	2.209	Pb–N	2.682 (6)	C(1)–Si(1)	1.868 (8)	C(2)–B(3)	1.579 (10)
Pb–C(1)	2.712 (7)	Pb–C(2)	2.730 (8)	C(2)–B(6)	1.724 (10)	C(2)–Si(2)	1.878 (8)
Pb–B(3)	2.532 (12)	Pb–B(4)	2.451 (10)	B(3)–B(4)	1.702 (14)	B(3)–B(6)	1.779 (11)
Pb–B(5)	2.537 (8)	C(1)–C(2)	1.494 (12)	B(4)–B(5)	1.674 (14)	B(4)–B(6)	1.741 (13)
C(1)–B(5)	1.559 (11)	C(1)–B(6)	1.756 (13)	B(5)–B(6)	1.777 (17)		
Bond Angles							
Compound IV							
Cnt(1)–Ge(1)–N(1)	130.0	Ge(1)–N(1)–C(133)	109.2 (3)	Cnt(2)–Ge(2)–N(2)	128.0	Ge(2)–N(2)–C(233)	115.2 (3)
Ge(1)–N(1)–C(134)	110.4 (4)	Ge(1)–N(1)–C(135)	109.5 (4)	Ge(2)–N(2)–C(234)	103.1 (4)	Ge(2)–N(2)–C(235)	110.7 (3)
C(12)–C(11)–B(15)	111.1 (4)	C(12)–C(11)–Si(11)	131.0 (4)	C(22)–C(21)–B(25)	112.1 (5)	C(22)–C(21)–Si(21)	129.3 (4)
B(15)–C(11)–Si(11)	117.9 (4)	B(16)–C(11)–Si(11)	137.7 (4)	B(25)–C(21)–Si(21)	117.9 (3)	B(26)–C(21)–Si(21)	131.9 (4)
C(11)–C(12)–B(13)	111.9 (5)	C(11)–C(12)–Si(12)	128.9 (3)	C(21)–C(22)–B(23)	111.7 (4)	C(21)–C(22)–Si(22)	130.7 (4)
B(13)–C(12)–Si(12)	118.8 (4)	B(16)–C(12)–Si(12)	133.7 (4)	B(23)–C(22)–Si(22)	117.5 (3)	B(26)–C(22)–Si(22)	135.0 (4)
C(12)–B(13)–B(14)	106.1 (4)	B(13)–B(14)–B(15)	104.4 (5)	C(22)–B(23)–B(24)	106.4 (5)	B(23)–B(24)–B(25)	103.5 (5)
C(11)–B(15)–B(14)	106.3 (5)	N(1)–C(133)–C(123)	113.8 (5)	C(21)–B(25)–B(24)	105.9 (4)	N(2)–C(233)–C(223)	112.6 (5)
Compound X(A)							
Cnt–Pb–N	124.3	Pb–N–C(23)	108.6 (4)	B(3)–B(4)–B(6)	62.2 (5)	B(5)–B(4)–B(6)	62.7 (6)
Pb–N–C(24)	114.3 (5)	Pb–N–C(25)	103.2 (4)	C(1)–B(5)–B(4)	107.0 (8)	C(1)–B(5)–B(6)	63.1 (6)
C(2)–C(1)–B(5)	111.5 (6)	C(2)–C(1)–B(6)	63.5 (5)	B(4)–B(5)–B(6)	60.5 (6)	C(1)–B(6)–C(2)	50.9 (5)
B(5)–C(1)–B(6)	64.5 (6)	C(2)–C(1)–Si(1)	130.5 (5)	C(1)–B(6)–B(3)	92.4 (5)	C(2)–B(6)–B(3)	53.5 (4)
B(5)–C(1)–Si(1)	117.6 (6)	B(6)–C(1)–Si(1)	135.4 (5)	C(1)–B(6)–B(4)	96.0 (7)	C(2)–B(6)–B(4)	97.5 (6)
C(1)–C(2)–B(3)	112.2 (6)	C(1)–C(2)–B(6)	65.7 (5)	B(3)–B(6)–B(4)	57.8 (5)	C(1)–B(6)–B(5)	52.4 (5)
B(3)–C(2)–B(6)	65.0 (5)	C(1)–C(2)–Si(2)	129.0 (5)	C(2)–B(6)–B(5)	92.3 (6)	B(3)–B(6)–B(5)	97.0 (7)
B(3)–C(2)–Si(2)	118.2 (6)	B(6)–C(2)–Si(2)	131.1 (6)	B(4)–B(6)–B(5)	56.8 (6)	N–C(23)–C(13)	110.8 (6)
C(2)–B(3)–B(4)	105.0 (7)	C(2)–B(3)–B(6)	61.4 (4)	C(23)–N–C(24)	110.6 (6)	C(23)–N–C(25)	110.9 (7)
B(4)–B(3)–B(6)	60.0 (5)	B(3)–B(4)–B(5)	104.1 (6)	C(24)–N–C(25)	109.0 (7)		

[a] Cnt = centroids of C_2B_3 rings.

Table VI. Mean Deviations (Å) and Dihedral Angles (deg) of the Least-Squares Planes for IV and X(A)

Mean Deviations

plane	complex IV molecule 1	complex IV molecule 2	complex X(A)
1 (C_2B_3 ring)	0.024	0.031	0.021
2 (Cp(1) ring)	0.002	0.003	0.002
3 (Cp(2) ring)	0.002	0.002	0.004

Dihedral Angles

planes	complex IV molecule 1	complex IV molecule 2	complex X(A)
1 and 2	70.3	96.9	78.2
1 and 3	69.9	96.9	78.7
2 and 3	0.8	0.2	0.7

structure of IV. On the other hand, in the base–plumbacarborane system, the melting point of compound XII, which has the lowest molar mass in the series, is significantly higher than that of either X or XI. This could indicate that XII is polymeric. The fact that crystals of XII do not give good X-ray diffraction patterns is also consistent with possible polymeric or oligomeric formation. However, neither the solution NMR nor IR spectra of XII show abnormalities that require the assumption of extended molecular association.

Characterization. Compounds IV–VI and X–XII were characterized by ^1H, ^{11}B, and ^{13}C pulse Fourier transform NMR (Table I), IR (Table II), and mass spectroscopy (supplementary table S-1). Compounds IV and X were also characterized by X-ray diffraction studies (Tables III–VI).

Mass Spectra. High-resolution electron impact (HREI) mass spectra were obtained for compounds IV–VI and X–XII. All showed only the corresponding parent groupings, with the exception of V, which also showed a weak signal corresponding to the parent grouping plus a proton. The relatively simple mass spectra of these compounds indicate fairly strong bonding between the ferrocene amine and the metallacarboranes.

NMR and IR Spectra. The IR spectra (Table II) and the ^1H, ^{11}B, and ^{13}C NMR spectra (Table I) of the compounds show the presence of the carborane cage and ferrocene amine base and are all consistent with the formulas given in the Experimental Section. Changes in the ^{11}B and ^{13}C chemical shifts as one goes from the metallacarboranes (I–III and VII–IX) to their respective donor–acceptor complexes (IV–VI and X–XII) are similar to those reported for the ferrocene amine–stannacarborane complex[7] and are typical of those found in the formation of other pentagonal-bipyramidal metallacarborane–base complexes.[3-8,11,12] The apical ^{11}B resonances are the most sensitive to changes in complexation of the cage. In the uncomplexed nido dianion the apical boron resonance occurs at about −45 ppm (relative to $BF_3{\cdot}OEt_2$);[21] complexation with the metal causes it to shift downfield by about 40 ppm (δ(I) is −1.5 ppm,[11] and δ(VII) is 2.0 ppm[12]). This shift has been explained in terms of a decrease in the electron density on

(21) Barreto, R. D.; Hosmane, N. S. *Inorg. Synth.*, in press.

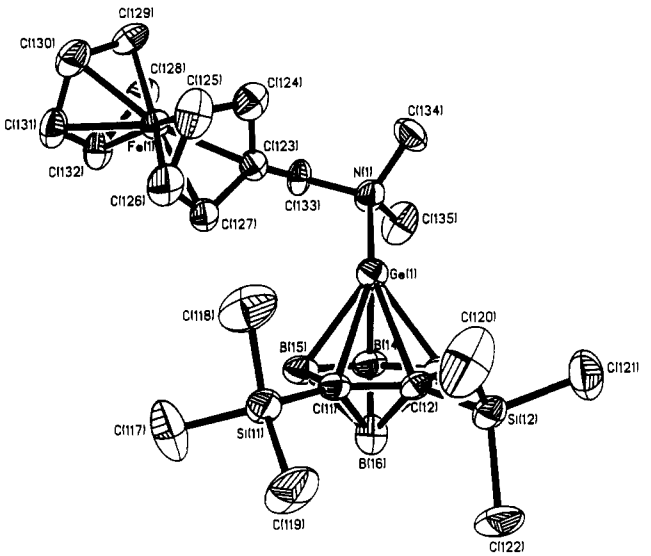

Figure 1. Perspective view of 1-Ge[(η^5-C_5H_5)Fe(η^5-$C_5H_4CH_2$-$(Me)_2N$)]-2,3-$(SiMe_3)_2$-2,3-$C_2B_4H_4$ (IV) showing the atom-numbering scheme. The thermal ellipsoids are drawn at the 40% probability level.

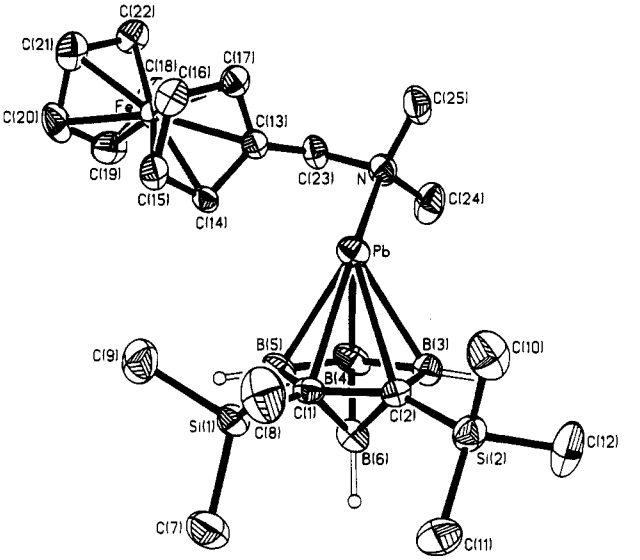

Figure 2. Perspective view of 1-Pb[(η^5-C_5H_5)Fe(η^5-$C_5H_4CH_2$-$(Me)_2N$)]-2,3-$(SiMe_3)_2$-2,3-$C_2B_4H_4$ (X(A)) showing the atom-numbering scheme. The thermal ellipsoids are drawn at the 40% probability level.

the apical boron when the carborane bonds to the metal.[20] Since both the metal and the apical boron compete with one another for the π-type electrons in the C_2B_3 pentagonal face of the carborane, any interaction that causes, or strengthens, metal–carborane bonding will polarize electron density away from the apical boron. Therefore, complexation of the metal by another base will be at the expense of metal–carborane bonding and will, to some extent, tend to restore electron density back toward the apical boron. Thus, coordination of the metal with a base, such as ferrocene amine, should cause a shift of the apical boron resonance back upfield. A comparison of the apical boron chemical shifts listed in Table I with those of the uncoordinated metallacarboranes[11,12] shows that this is the case. Heřmánek and co-workers[22] have studied the ^{11}B NMR spectra of compounds of the form $EB_{11}H_{11}$ and EB_9H_9 as a function of E (E = cage moiety bonded through a group 13, 14, 15, or 16 atom). They found that the variation with E of the chemical shift of the boron atom opposite to E is more a function of the population of the tangential p orbitals of E than the gross electron density of the atom. A theoretical and experimental NMR study of a series of base–metallacarborane complexes is currently under way in our laboratories with the aim of obtaining structure information from NMR data. However, at this point, structural details of the base–metal–carborane systems are accessible only through X-ray diffraction.

Crystal Structures of 1-Ge[(η^5-C_5H_5)Fe(η^5-$C_5H_4CH_2(Me)_2N$)]-2,3-$(SiMe_3)_2$-2,3-$C_2B_4H_4$ (IV) and 1-Pb[(η^5-C_5H_5)Fe(η^5-$C_5H_4CH_2(Me)_2N$)]-2,3-$(SiMe_3)_2$-2,3-$C_2B_4H_4$ (X) and Molecular Orbital Analysis. The structures of IV and X were determined by single-crystal X-ray diffraction and show the structures depicted in Figures 1 and 2. These structures are quite similar to that found for the corresponding tin complex.[7] Indeed, X(B) is essentially isomorphic with the tin complex (see supplementary figure S-2B). In all molecules the ferrocene amine base bonds to the metallacarborane primarily through the nitrogen atom of the base. The metal resides above the C_2B_3 open face of the carborane and is slipped toward the boron side of that face. A comparison of the lead–carborane atom distances in the uncomplexed plumbacarborane[12] with those in X show that, after complexation with the ferrocene amine base, the Pb–B(4) bond distance decreased by about 0.1 Å, indicating an increased slip distortion on coordination with the base. An increase in the slip distortion of the capping metal of a main-group metallacarborane on complexation with a Lewis base is a common feature of the chemistry of these compounds.[2] From Table VI, which lists the mean deviations from planarity of the Cp and C_2B_3 rings and the dihedral angles of the Cp and C_2B_3 planes, it is apparent that the Cp rings are planar and parallel to one another, while the C_2B_3 faces show substantially higher deviations from planarity. This is due primarily to the fact that there is a slight folding of the C_2B_3 face along the B(3)–B(5) line of about 6°, causing B(4) to be directed slightly below the B(3)–C(1)–C(2)–B(5) plane. Such ring folding has been observed in a number of metallacarboranes.[5,23,24]

The unit cells of both IV and X(B) contain two crystallographically independent molecules, designated as IV(1), IV(2) and X(B1), X(B2), respectively. The isomers differ in the relative orientations of the carborane and ferrocene amine ligands. In isomer 1, the M–N bond lies in the mirror plane of the MC_2B_4 cage, that is, the plane defined by M, B(4), B(6), and the midpoint of the C(1)–C(2) bond (see Figures 1 and 2), while in isomer 2 the bond is slightly rotated out of the plane; in IV(2) the Ge–N bond makes an angle of 9° with this plane, and in X(B2) the Pb–N angle is 12°. The structure of X(A) is similar to that of isomers 2 in that the corresponding angle is 12° (see Figure 2). Inspection of Table IV shows that the bond distances in isomers IV(A) and IV(B) are about the same, with the largest differences being found in the germanium-containing bonds. However, even these differences are generally less than 0.1 Å. Similar differences are found in the corresponding stannacarborane– and plumbacarborane–ferrocene amine complexes (see ref 7 and supplementary table S-4). Table VI shows that as one goes from isomers 1 to 2 the dihedral angles between the Cp and C_2B_3 planes increase by about 26–27°, resulting from

(22) Heřmánek, S.; Hnyk, D.; Havlas, Z. *J. Chem. Soc., Chem. Commun.* **1989**, 1859.

(23) Colquhoun, H. M.; Greenbrough, T. J.; Wallbridge, M. G. H. *J. Chem. Soc., Dalton Trans.* **1985**, 761.

(24) Hosmane, N. S.; Zhang, H.; Lu, K.-J.; Maguire, J. A.; Cowley, A. H.; Mardones, M. A. *Struct. Chem.*, in press.

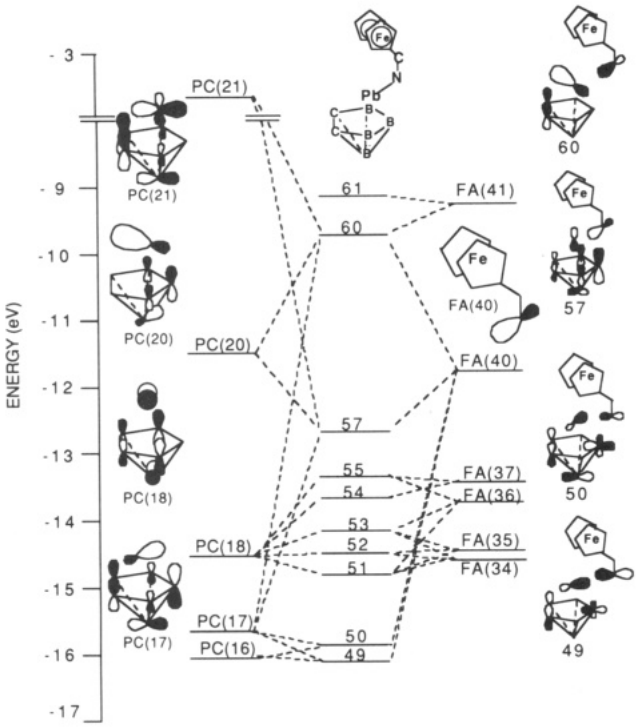

Figure 3. Molecular orbital correlation diagram for XIV in terms of its $PbC_2B_4H_6$ and ferrocene amine fragment orbitals and sketches giving the heavy-atom compositions of some of the important complex and fragment orbitals.

a slight rotation of the ferrocenyl group about the C(23)–C(33) bond in IV (see Figure 1). However, this rotation does not seem to materially alter the distance between the metal and the ferrocene group; the Ge–C(23) bond lengths, which represent the distance of closest approach, are the same in the two isomers of IV. The same is true for the two isomers of X(B).

Fenske-Hall molecular orbital calculations were carried out on the model compounds XIII–XV. Each complex has 61 filled molecular orbitals constructed from the valence orbitals of their respective atoms. Of these, 10 have sufficient metal, carborane, and base character to be considered important in understanding the bonding of the metal to the carborane and ferrocene amine ligands. The genesis of these orbitals is seen in Figure 3, which shows the molecular orbital correlation diagram of XIV in terms of its plumbacarborane and ferrocene amine fragment orbitals. Since the bondings in XIII–XV are quite similar, Figure 3 is also qualitatively correct for both XIII and XV. Because of the similarities in these complexes, only the plumbacarborane complex (XIV) will be discussed in detail; unless otherwise noted, what is said for XIV can be equally applied to XIII or XV. In the construction of the molecular orbitals a coordinate system was used such that the mirror plane of the $PbC_2B_4H_6$ fragment constituted the xz plane and the unique boron, B(4) in Figures 1 and 2, was situated on the x axis. A local coordinate system was defined for the ferrocene moiety so that the z axes of the Cp carbon atoms were perpendicular to the plane of the particular Cp ring and in the direction of the iron. These coordinate definitions yield fragment and adduct molecular orbitals that can be directly compared to those of other group 14 metallacarboranes[7,11] and the well-known metallocene MO's.[25] Compounds XIII–XV model only the more symmetric isomers of the ferrocene amine com-

(25) Shriver, D. F.; Atkins, P. W.; Langford, C. H. *Inorganic Chemistry*; W. H. Freeman: New York, 1990; Chapter 16, pp 522–525.

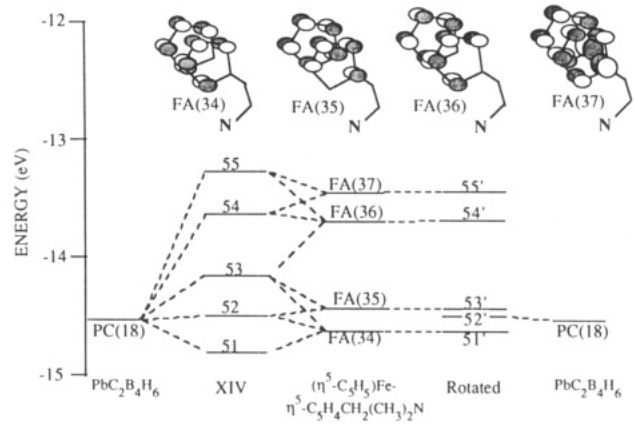

Figure 4. Heavy-atom compositions of some ferrocene amine fragment orbitals and a partial molecular orbital correlation diagram of XIV showing their interactions with PC(18) before and after rotation of the ferrocene group by 120°. For clarity, the iron orbitals are not shown.

plexes, where the base nitrogen is in the mirror plane of the metallacarborane. The higher symmetry of these isomers somewhat simplifies the resulting MO's (see supplementary tables S-10–S-12 for the atomic orbital populations of the MO's of XIII–XV). The $PbC_2B_4H_6$ fragment has 20 filled MO's, designated as PC(1)–PC(20), and the ferrocene amine fragment has 41 filled MO's (FA(1)–FA(41)). These give rise to the 61 filled MO's for the adduct. Figure 3 also shows the sketches of some of the more important fragment and complex orbitals in terms of their input atomic orbitals. The six highest energy ferrocene amine MO's, FA(34)–FA(41), are the ones primarily involved in bonding to the metallacarborane. Fragment orbital FA(40) is localized on the nitrogen (82%) and is directed away from the other groups bonded to this atom; this is the lone-pair orbital of the base (see Figure 3). The other five ferrocene amine fragment orbitals are localized on the ferrocenyl group of the base and account for the bonding between the Fe(d) orbitals and the Cp(π) MO's. The descriptions of these fragment orbitals is as follows. FA(41) is 90% Fe($3d_{z^2}$) and corresponds to the $4a_1'$ ferrocene MO;[25] it constitutes the majority (91%) of the HOMO of XIV (MO 61). FA(37) and FA(36) are derived from the ferrocene's degenerate $3e_2''$ MO's, which involve Cp(π)–Fe($4p_x$,$4p_y$) bonding and are localized on the Cp carbons. FA(35) and FA(34) are derived from the $3e_1''$ MO of ferrocene, which involves Cp(π)–Fe($3d_{xz}$,$3d_{yz}$) bonding. Sketches of FA(34), FA(35), FA(36), and FA(37) are shown in Figure 4. As can be seen from Figure 3, the metallacarborane fragment orbitals that interact strongly with the base are also those that give rise to strong metal–carborane bonding. The important PC fragment orbitals are also sketeched in Figure 3. Plumbacarborane fragment orbitals PC(21), PC(20), and PC(17) are symmetric with respect to the mirror plane of the fragment and interact strongly with the lone-pair base orbital (FA(40)). In plumbacarborane fragment orbital PC(21), the LUMO of the metallacarborane fragment, the lead and carbon atoms are antibonding to one another; PC(21) is localized on the Pb(p_z) (65%) and the C_{cage}(p_z) (8%) orbitals. The contribution of this virtual metallacarborane fragment orbital is important in rationalizing the large metal slip distortion found in the adduct molecules. In PC(20) and PC(17) the metal and carborane orbitals are generally bonding; PC(20) is localized on the lead (72%) and B(4) (12%), while PC(17) is more localized on the cage carbons (30% Pb, 28% C_{cage}, and 16% B(4)). These three symmetric metallacarborane fragment orbitals interact extensively with the

Table VII. Metal–Carborane Mulliken Overlap Populations Calculated for XIII–XV and Their Metallacarborane Fragments

species	metal	Mulliken overlap populations C(1/2)[a]	B(3/5)[a]	B(4)[a]
$GeC_2B_4H_6$	Ge	0.1891	0.3604	0.3893
XIII	Ge	0.0668	0.3515	0.3896
$PbC_2B_4H_6$	Pb	0.1642	0.3191	0.3309
XIV	Pb	0.0442	0.3133	0.3186
$SnC_2B_4H_6$	Sn	0.1692	0.3291	0.3340
XV	Sn	0.0624	0.3178	0.3261

[a] See Figures 2 and S-2B (supplementary material) for atom-numbering system.

lone-pair base orbital, FA(40), to form the primary metallacarborane–base bonding. Since these metallacarborane orbitals are also involved in metal–carborane bonding, metal–base bonding is accomplished at the expense of metal–carborane bonding. However, the decrease in the metal–carborane atom bonding is not distributed equally among the C_2B_3 face atoms. This can be seen from the Mulliken overlap populations[26] (MOP) of the metal and the C_2B_3 face atoms in XIII–XV and their respective metallacarborane fragments that are listed in Table VII. As can be seen from this table, for the germanium, lead, and tin complexes there is a large decrease in the metal–cage carbon bonding, as measured by MOP's, when the metallacarborane forms a complex with the ferrocene amine base. On the other hand, the MOP's indicate that bonding to the boron atoms is much less affected. An analysis of the various orbital–orbital populations shows a diminution of the MOP's of metal s and p_x orbitals with the cage carbon p_z (p_π) orbitals on complexation with base. This can be traced to the contribution of PC(21) in MO's 60 and 57. Adduct MO(60) is composed of the metallacarborane fragment orbitals PC(21) (13%) and PC(20) (55%) and the lone-pair base orbital, FA(40) (18%). Because of the mixing of PC(21) and PC(20) in this MO, the metal and cage carbons are antibonding, while the metal–base interactions are generally bonding. Therefore, occupation of this molecular orbital, while promoting metal–base bonding, will detract from metal–carborane bonding, especially metal–cage carbon bonding. On the other hand, adduct MO(57), in which the metal is strongly bonding to both the carborane borons and base, is 30% PC(20), 22% PC(17), 7% PC(21), and 33% FA(40) and is more heavily localized on the boron atoms than on carbon. Therefore, complexation of the metallacarborane with the base detracts more from metal–carbon bonding than it does from metal–boron bonding; this should encourage an increase in the slip distortion of the metal. Since similar interactions were found to be important in accounting for the slip distortion found in group 13 and 14 metallacarborane complexes with bidentate bases,[5,20,23,24,27] this is not a unique property of the monodentate ferrocene amine base. What is important is the relative orientation of the base and the carborane ligands. The base preferentially weakens bonds opposite to it in the complex. For the group 14 metallacarborane–base complexes the base resides over the facial boron atoms and the slippage is away from the cage carbons (See Figures 1 and 2 and ref 7 and 9). This same general rule seem to be operative in homonuclear π complexes, such as the main-group cyclopentadienide system. The structures of $(C_5H_5)SnCl$[28] and $[(C_5H_5N)SnC_5Me_5]CF_3SO_3$[29] show the base ($C_5H_5N$ or Cl) above a Cp C–C bond midpoint, and the Sn is η^2-bonded to the Cp ligand. On the other hand, in $[(C_{10}H_8N_2)SnC_5Me_5]^+$ the bipyridine molecule is directly over one of the Cp carbons and the Sn is η^3-bonded to the Cp.[29]

Fragment orbital PC(18), the only major metal-containing orbital that is antisymmetric with respect to the metallacarborane fragment's mirror plane, is localized on the metal (30% Pb(p_y)) and basal borons (19% B(3/5)(p_z)) rather than the cage carbons (8% C(1/2)(p_z)) (see Figure 3). In isomers XIII–XV it cannot interact with the nitrogen lone-pair electrons on the base. However, Figure 3 shows that PC(18) does interact with ferrocene amine orbitals FA(34)–FA(37) to yield adduct orbitals MO(51)–MO(55). The compositions of these orbitals are as follows: MO(51), 25% PC(18), 66% FA(34), and 4% FA(35); MO(52), 5% PC(18), 15% FA(34), and 77% FA(35); MO(53), 48% PC(18), 18% FA(34), 17% FA(35), and 14% FA(36); MO(54), 8% PC(18), 71% FA(36), and 17% FA(37); MO(55), 13% PC(18), 70% FA(37), and 10% FA(36). None of these ferrocene amine orbitals contain nitrogen character (see supplementary tables S-10–S-12 and Figure 4), and the metal–base interactions seem to be through the metal p_y orbital and the Cp(π) electrons of the ferrocenyl group. Figure 4 shows the changes in $PbC_2B_4H_6$–ferrocene amine interactions in XIV when the ferrocenyl group is rotated by 120° around the equivalent of the C(23)–C(13) bond shown in Figure 2. Such a rotation would move the ferrocene moiety away from the lead atom so that the distance of closest approach of a ferrocene atom to lead is 4.73 Å, rather than the 3.2 Å found in X(A) and X(B), but would keep all other important internuclear distances the same. As can be seen from Figure 4, rotation of the ferrocene completely removes any interactions between PC(18) and the ferrocene amine orbitals FA(34)–FA(37); lead–base bonding is then exclusively through the nitrogen lone-pair orbital (FA(40)). Similar calculations on XIII and XV show essentially the same results; that is, the main metal–base bonding is through the interaction of the nitrogen lone-pair orbital and a series of metal-centered orbitals that are symmetric to the mirror plane of the metallacarborane. However, there are additional interactions between the metal and Cp(π) orbitals, which disappear when the ferrocene is rotated away from the metal. The main difference found as one goes from lead to the smaller tin and germanium atoms is that, as the size of the metal decreases, there is an increasing interaction between the ferrocene amine orbitals FA(37) and FA(36) and orbitals equilvalent to PC(20); these interactions cease on rotation of the ferrocene. Since total energies cannot be obtained from the calculation method used, it is impossible to ascertain to what extent, if any, these secondary metal–Cp(π) interactions stabilize the donor–acceptor adduct. From the small orbital energy changes seen in Figures 3 and 4, it is apparent that the contributions of these interactions to the overall stability are small. However, they do provide an explanation of the sterically unfavorable orientation of the ferrocenyl group in the adducts. Since this interaction does involve the direct transfer of electron density from the ferrocenyl Cp to the metal, it could also account for the unusual chemical shift of the ^{119}Sn NMR resonance on complexation with ferrocene amine.[7] If this is so, then the chemical shift anomaly should be removed if the ferrocene is in a more sterically preferred position

(26) Mulliken, R. S. *J. Chem. Phys.* **1962**, *36*, 3428.
(27) Barreto, R. D.; Fehlner, T. P.; Hosmane, N. S. *Inorg. Chem.* **1988**, *27*, 453.
(28) Boz, K. D.; Bulten, E. J.; Noltes, J. G. *J. Organomet. Chem.* **1975**, *99*, 71.
(29) Kohl, F. X.; Schlüter, E.; Jutzi, P.; Krüger, C.; Wolmerschänser, G.; Hofman, P.; Staufert, P. *Chem. Ber.* **1984**, *117*, 1178.

in a tin-ferrocene amine complex. We are currently investigating the chemical shift-structure relationships in a number of different stannacarboranes to see if this is indeed the case.

Acknowledgment. This work was supported by grants from the National Science Foundation (CHE-9100048), the Robert A. Welch Foundation (N-1016), and the donors of the Petroleum Research Fund, administered by the American Chemical Society. We thank Dr. Anil Saxena for his assistance during the synthesis of germanium adducts. The help and assistance of Professor T. P. Fehlner of the University of Notre Dame and Dr. R. L. Cerny and Mr. C. Jacoby of the Midwest Center for Mass Spectrometry, a National Science Foundation Regional Instrumentation Facility (Grant No. CHE-8211164), is also gratefully acknowledged.

Supplementary Material Available: Mass spectrometric data (Table S-1) for IV-VI and X-XII, a summary of crystallographic data for IV, X(A), and X(B) (Table S-2), atomic coordinates for X(B) (Table S-3), bond lengths and angles for IV, X(A), and X(B) (Table S-4), anisotropic displacement coefficients for IV, X(A), and X(B) (Table S-5), H atom coordinates and isotropic displacement coefficients for IV and X(A) (Table S-6), a perspective view of X(B) (Figure S-2B) showing the atom numbering scheme, and compositions of the molecular orbitals in compounds XIII (Table S-10), XIV (Table S-11), and XV (Table S-12) (61 pages). Ordering information is given on any current masthead page.

OM9107146

Synthesis and Structural Characterization of the Isomers of (1-Phosphino-η^3-pentenyl)tricarbonylmanganese

Ma. Angeles Paz-Sandoval,* Patricia Juárez Saavedra, Noé Zúñiga Villarreal, Ma. Jesús Rosales Hoz, and Pedro Joseph-Nathan

Departamento de Química, Centro de Investigación y de Estudios Avanzados del Instituto Politécnico Nacional, Apartado 14-740, México, D.F. 07000, México

Richard D. Ernst and Atta M. Arif

Department of Chemistry, University of Utah, Salt Lake City, Utah 84112

Received November 26, 1991

Diphenylphosphine reacts with η^5-pentadienyltricarbonylmanganese (1) to give isomers Mn[P(Ph)$_2$CH$_2$-η^3-CHCHCHCH$_3$](CO)$_3$ (2) and Mn[P(Ph)$_2$CH$_2$CH$_2$-η^3-CHCHCH$_2$](CO)$_3$ (3). In both cases, phosphorus is added stereoselectively to the terminal carbon atom. Single-crystal X-ray diffraction studies of 2 and 3 confirm the unprecedented formation of the novel [1-(diphenylphosphino)-η^3-pentenyl]tricarbonylmanganese complexes in which the phosphahexenyl ligand is bonded to the manganese center through an η^3 interaction and also by phosphorus coordination affording six- and seven-membered "pseudo"-ring structures. Crystals of 2 are orthorhombic, space group $Pna2_1$ with a = 8.844 (1) Å, b = 16.806 (2) Å, c = 12.629 (1) Å, and Z = 4. The structure was refined to discrepancy indices of R = 0.0596 and R_w = 0.0602 for 1468 reflections having $I > 3\sigma(I)$. Crystals of 3 are monoclinic, space group $P2_1/a$, with a = 10.630 (7) Å, b = 11.979 (8) Å, c = 14.27 (1) Å, β = 92.32 (6)°, and Z = 4. The structure was refined to discrepancy indices of R = 0.0641 and R_w = 0.0712 for 1735 reflections having $I > 3\sigma(I)$. The two complexes have distorted-octahedral geometries with important differences both in lengths within the phosphino-η^3-pentenyl systems and for the bonding parameters of the manganese ions. The metal carbonyl distances also show significant differences from one complex to the other. Monitoring of the reaction by IR and NMR (^{31}P, ^{1}H) spectroscopy showed that the addition of PHPh$_2$ to 1 proceeds by initial conversion to 2 and subsequent formation of 3, with no evidence for preliminary interaction at either the manganese center or one of the CO carbon atoms. The reactions of *cis*-MnBr(CO)$_4$PHPh$_2$ (7a) and *fac*-MnBr(CO)$_3$(PHPh$_2$)$_2$ (8a) with C$_5$H$_7$SnBu$_3$ to initially afford compound 2, are also discussed. The crystal of 7a is monoclinic, space group $P2_1/c$ with a = 11.325 (5) Å, b = 10.342 (3) Å, c = 14.813 (5) Å, β = 95.08 (3)°, and Z = 4. The structure was refined to values of R = 0.0495 and R_w = 0.0540 for 2001 reflections with $I > 3\sigma(I)$. The complex has a pseudooctahedral geometry with the bromine and diphenylphosphine ligands cis to each other.

Introduction

We recently described[1] studies on the reactivity of C$_5$H$_7$Mn(CO)$_3$ with secondary amines, the results of which support the occurrence of a 1,5-addition of the -NH function to the pentadienyl ligand, followed by coordination of the nitrogen atom to the manganese center and ultimately affording (1-amino-1-3-η^3-pentenyl)tricarbonylmanganese complexes. In order to clarify the key factors that determine the reactivity patterns in C$_5$H$_7$Mn(CO)$_3$, we turned to the study of diphenylphosphine to explore how the PH function would act on the pentadienyl fragment. In this regard, the reactivity of complexes such as LM(CO)$_n$ [n = 3: M = Mn, L = Cp;[2] M = Mn, L = cycloheptadienyl;[3,4] M = Mn, Fe$^+$, L = cyclohexadienyl,[4] pentadienyl,[5] oxopentadienyl.[6] n = 4: M = Mn, L =

(1) Zúñiga Villarreal, N.; Paz-Sandoval, M. A.; Joseph-Nathan, P.; Esquivel, R. O. *Organometallics* **1991**, *10*, 2616.

(2) Caulton, K. G. *Coord. Chem. Rev.* **1981**, *38*, 1.

(3) (a) Hong, E. D.; Sweigart, D. A. *J. Chem. Soc., Chem. Commun.* **1986**, 691. (b) Haque, F.; Miller, J.; Pauson, P. L.; Tripathi, J. B. *J. Chem. Soc. C* **1971**, 743.

(4) Gower, M.; John, G. R.; Kane-Maguire, L. A. P.; Odiaka, T. I.; Salzer, A. *J. Chem. Soc., Dalton Trans.* **1979**, 2003 and references therein.

0276-7333/92/2311-2467$03.00/0